Electronic and thermoelectric properties of ZrS_xSe_{2-x}

A. Ghafari[1,2], C. Janowitz[3]

[1]*Helmholtz-Zentrum Berlin für Materialien und Energie GmbH, Hahn-Meitner-Platz 1, 14109 Berlin, Germany*

[2] *Department of Inorganic Chemistry, Fritz-Haber-Institut der Max-Planck-Gesellschaft, Faradayweg 4-6, 14195 Berlin, Germany*

[3]*Humboldt Universität, Institut für Physik, Newtonstr. 15, 12489 Berlin, Germany*

Abstract

The electronic, phonon, and transport properties of ternary ZrS_xSe_{2-x} (x=0, 1, and 2) have been calculated based on density functional theory (DFT), density functional perturbation theory (DFPT), and Boltzmann transport theory. Two methods for engineering of the electronic and transport properties of ternary ZrS_xSe_{2-x} (x=0, 1, and 2) shall be treated: (i) doping which can be achieved by the help of the rigid band approximation could be valid for the low doping levels of n- and p-type of ZrS_xSe_{2-x} (x=0.1, 2). (ii) The substitution of S by Se in ZrS_xSe_{2-x} (x=0.1, 2). Here, both methods have been applied to engineer the bandgap and power factor. This enables us to look at the optimal power factor and figure of merit for the n- and p-type doped ternary ZrS_xSe_{2-x} (x=0, 1, and 2). It has been found that the p-doped $ZrSe_2$ has the highest power factor and the lowest bandgap between three compounds while the highest Seebeck coefficient is observed in ZrS_2. But the highest figure of merit (ZT) is found in ZrSeS which has the lowest lattice thermal conductivity such that at 300 K it is about 0.33 and 0.32 for the n- and p-doped, respectively. The minimum total thermal conductivity has also been obtained in ZrSeS which is 0.61 and 0.18 along the a- and c-directions, respectively at 1000 K. This value of the lattice thermal conductivity along the c-axis is even lower than the reported value for the well-known low lattice thermal conductivity of SnSe [L.D. Zhao, et al. Nature, **508**, 373 (2014)].

1. Introduction

Thermoelectric (TE) materials which are a topic of renewed interest could play a basic role for harvesting enormous amounts of waste heat [1,2]. The efficiency of TE materials is determined by the dimensionless figure of merit ZT which is defined as $ZT=(S^2\sigma/\kappa)T$. Where T is the temperature and S, σ, and κ are the Seebeck coefficient, the electrical conductivity and the thermal conductivity provided by the electrons and phonons (i.e. $\kappa=\kappa_e+\kappa_l$), respectively. These quantities are strongly interrelated which makes a real challenge for enhancing of the figure of merit. For increasing of the TE performance one could engineer the transport properties which can be achieved by doping in the crystal structure. This can be done by substitution of an element in the compound by another element. In addition within the rigid band approximation [3] the Fermi level position is defined in the fundamental gap of the n-and-p doped compounds.

It should be noted that the rigid band approximation which is valid for the low doping level has been widely used [4,5]. Then, using the Boltzmann transport equation [6,7] it could be possible to engineer the transport properties in order to obtain the maximum TE performance in a compound. For this purpose, the power factor in the n-and p-doped regime can calculated. From that the maximum power factor for the n- and p- doping can be obtained. This enables us to look at the temperature dependence of transport properties at the optimal n- and p-doping level of each compound.

Zirconium dichalcogenide compounds have attracted much interest due to their suitability for a number of applications. For instance, in the ternary ZrS_xSe_{2-x} (x=0, 1, 2) compounds it has been obtained that the band gap can be engineered [8–13] which could be interesting for the third-generation photovoltaic applications as discussed in [1]. Moreover, the spin-orbit (SO) splitting of the valence band maximum (VBM) has been observed experimentally [9,10,13] and theoretically [11,12]. This finding could also be interesting because the SO splitting produces multiple separated valley pockets of the Fermi surface therewith influencing the transport properties. These observations give a strong motivation to

investigate the transport properties and the TE performance of ZrS_xSe_{2-x} (x=0, 1, 2) in the optimal p- and n-doping regime.

In this paper, these three methods (i.e. the rigid band approximation, the substitution of S by Se in ZrS_xSe_{2-x} (x=0.1, 2), and the maximum power factor at the n- and p- doping of each compounds) are used in order to engineer the transport properties in the ternary ZrS_xSe_{2-x} (x=0, 1, 2) compounds. For this purpose, by presenting the band structure and phonon dispersion, the transport properties of ZrS_xSe_{2-x} (x=0, 1, 2) (i.e. the Seebeck S, the electron and the lattice thermal conductivity (κ_e, κ_l), the powerfactor, and the figure of merit ZT) are investigated. Moreover, by looking at the n- and p-type doped regime the temperature dependence of transport properties and the TE performance at the optimal n- and p-type doped of ZrS_xSe_{2-x} are discussed.

2. Computational methods

The crystal structure of ZrS_xSe_{2-x} is from the family of the transition metal dichalcogenides (TMDC) with formula MX_2 (M= transition metal, X=chalcogenide). It consists of a sheet of metal atom sandwiched between two sheets of chalcogens which forming a trilayer of X-M-X with a thickness of about 6~7 Å. The strong covalent bonds inside the layers exist while relatively weak van der Waals forces hold the sheets together. ZrS_2 and $ZrSe_2$ have the P-3m1 (Nr. 164) space group while ZrSeS has the P3m1 space group [14]. The atomic positions in the structures are $ZrSe_2$: Zr at (0 0 0), Se at (0.66 0.33 0.75) and (0.33 0.66 0.25); ZrSeS: Zr at (0 0 0), Se at (0.66 0.33 0.75), and S at (0.33 0.66 0.25); ZrS_2: Zr at (0 0 0), S at (0.66 0.33 0.75) and (0.33 0.66 0.25).

The band structure and density of states (DOS) have been calculated by the Wien2k code [15] using the theoretical lattice constants ($ZrSe_2$: a=3.789 Å, c=6.165 Å; ZrSeS; a=3.713 Å, c=6.010 Å; ZrS_2: a=3.654 Å, c=5.795 Å) with 600 k-points mesh in the Brillouin zone (BZ). This is corresponding to the k-spacing of $0.10\ Å^{-1}\ and\ 0.11\ Å^{-1}$ along the a and c-axis, respectively. The theoretical lattice

constants have been obtained by relaxation of the experimental asymmetric cells in the PBEsol functional [16]. Moreover, in the calculations the G_{max}=14 (a.u.)$^{-1}$ (the largest vector in the charge density Fourier expansion), and $R_{MT}K_{max}$=8.5 where $R_{MT}K_{max}$ presents the smallest muffin-tin radius R_{MT} times the largest k-vector k_{max} (the plane-wave expansion of the wave function) have been considered.

Using QUANTUM-ESPRESSO package [17] the phonon spectra (with 4×4×4 q-points), anharmonic scattering coefficients (with 3×3×2 q-points) [18–20], and the lattice thermal conductivity (by solving exactly the linearized Boltzmann transport equation with 12×12×12 k-points and smearing of 25 cm^{-1}) [6,7] have been calculated. Moreover, the ground-state calculations of phonon spectra have been performed with the norm-conserving pseudopotential using well-converged k-points sampling (i.e. 12×12×8) and 130 Ry (kinetic energy cutoff for the wave functions) with PBE functional [21]. The convergence test for k-points and smearing have been carefully performed. Boltzmann transport theory as implemented in the BoltzTraP code [22] has been used for the calculations of the transport properties with 80000 k-points in the BZ using the experimental band gaps [9] while their ground state densities have been calculated by the MBJ potential [23] with the SO interaction.

3. Results and discussion

FIG. 1a-c shows the calculated band structure around the high symmetrical points of the BZ using the PBE0 hybrid functional [24] for x=0, 1, and 2. Here, the B3LYP [25,26] and PBE0 hybrid functionals are applied in order to compare the size of band gap with the MBJ functional. However, the former two methods are more expensive than the MBJ functional and it has been shown that the MBJ functional leads to good agreement with the experimental data [10–13,27,28] with respect to the generalized gradient approximations (GGA) functionals. All applied functionals in the three compounds reveal that the valance band maximum (VBM) and the conduction band minimum (CBM) are located at the Γ- and

L-points of the BZ, respectively while the CBM at the M-point is 191 meV, 195 meV, and 182 meV higher in energy for $ZrSe_2$, ZrSeS, and ZrS_2, respectively. It means that these three compounds are indirect gap semiconductor. Using the PBE0 functional the indirect energy gaps of 1.066 eV, 1.323 eV, and 1.594 eV are obtained respectively, for $ZrSe_2$, ZrSeS and ZrS_2 which are close to the ARPES data [9,13] (see table 1). The corresponding values by the B3LYP (MBJ-MBJSO) functional are 0.956 eV (0.927 eV-0.642 eV), 1.201 eV (1.297 eV-0.960 eV), and 1.452 eV (1.422 eV-1.255 eV), respectively. However, the corresponding values by optical absorption [8] (ARPES [9]) measurements are 1.18 eV (1.10 eV), 1.4 eV (-), and 1.70 eV (2.02 eV), respectively. These experimental and theoretical data reveal that the size of the band gaps of the ternary ZrS_xSe_{2-x} semiconductor series varies almost linearly with the composition parameter x. The impact of the engineered bandgap on the transport properties is discussed later. Furthermore, the VBM at the A-point shows a linear shift to higher binding energy which is located at -0.242 eV (-0.242 eV), -0.260 eV (-0.257 eV), and -0.392 eV (-0.389 eV), respectively for x=0, 1, and 2, with the PBE0 (B3LYP) hybrid functional. Additionally, the VB width calculated with the PBE0 (B3LYP) are 5.225 eV (5.038 eV), 5.164 eV (4.981 eV), and 5.139 eV (4.965 eV) for x=0, 1, and 2, respectively while for $ZrSe_2$ and ZrS_2 the reported ARPES data are (5.12 ± 0.1) eV and (4.5 ± 0.1) eV, respectively [10].

In table 1, our data and the experimental data (optical absorption measurements [2] and ARPES [3]) for the indirect band gap (at the Γ-L ($E_{\Gamma L}$) and Γ-M ($E_{\Gamma M}$)) are presented. Moreover, the direct band gap at the four points of the BZ (i.e. the Γ-, A-, L-, and M) with the B3LYP and PBE0 hybrid functionals as well as the MBJ potential (with SO and WSO coupling) are shown in table 2.

The reported optical absorption measurements of the direct band gap for $ZrSe_2$, ZrSeS and ZrS_2 are 1.61 eV, 1.80 eV, and 2.10 eV, respectively [8]. These are comparable to our calculations with the B3LYP (PBE0-MBJ) functional which are 1.655 eV (1.824 eV-1.349), 1.944 eV (2.126eV-1.640 eV),

and 2.161 eV (2.353 eV-1.850 eV), respectively (see table 2). It should be noted that for the TE applications as discussed in [29] the optimal band gap should be 6kBT (~151 meV) for the indirect gap semiconductors which has been calculated by assuming the parabolic band approximation while the value of $10k_BT$ (~252 meV) has been proposed by Mahan [30].

The DOS for x=0, 1, and 2 are presented in FIG. 1d-f in which the significant contribution of the Se/S and Zr to the VB- and CB- states can be observed. An analysis of the partial DOS (not shown) reveals that there is a strong hybridization in the three compounds between p states of S/Se and d states of Zr in which the p_x+p_y contribution in the S/Se is higher than that of p_z and also the contribution of $d_{xz}+d_{yz}$ is higher than that of the other Zr-d states. This strong in-plane hybridization makes strong covalent bonds inside the layers and weak van der Waals forces between the sheets.
The dispersion of the top three VBs at the Γ-point is shown in detail as calculated with PBE0, B3LYP, MBJ and MBJSO in FIG. 1g-i. It can be observed that: (i) since the VBs are mainly due to the p-states, the splitting of bands can be expected when the SO coupling is considered in the calculations. Due to the SO splitting one band shifts to the lower (higher) binding energy by about 32 meV (373 meV), 40 meV (197 meV), and 31 meV (55 meV) for x=0, 1, and 2, respectively. (ii) At the Γ-point the energy gap between the first and second VBM is increased when decreasing the atomic number of chalcogenide from $ZrSe_2$ to ZrS_2.

The phonon dispersions for x=0, 1, 2 around the high symmetrical points of the BZ are depicted in FIG. 1j-l. Since in the three compounds there are three atoms in the unit cell, then three acoustic branches and six optical branches are observed. The maximum frequencies of the acoustic branches are increased by decreasing the atomic number of the chalcogenide from $ZrSe_2$ to ZrS_2. The three compounds show almost similar dispersion curves for the acoustic branches around the high symmetrical points of the

BZ (see FIG. 1j-l). Here, we cannot compare our calculated phonon dispersions with experimental data due to the unavailable experimental phonon dispersions for the ternary ZrS_xSe_{2-x} (x=0, 1, 2). But one can compare our data with the experimental Raman spectra which consist of an in-plane E_g mode 145.5 cm^{-1} (250 cm^{-1}) and an out-of-plane vibrations A_{1g} mode 194.5 cm^{-1} (334.1 cm^{-1}) for $ZrSe_2$ (ZrS_2) [31] (see table 3). The corresponding values in our data are 149.36 cm^{-1} (253.61 cm^{-1}) and 193.29 cm^{-1} (338.50 cm^{-1}), respectively which show a good agreement [31]. Furthermore, in ZrSeS we have obtained the values of 199.79 and 239.43 for E_g and A_{1g}, respectively.

One important parameter for the transport properties is the relaxation time. In the BoltzTraP code [22] the transport properties based on constant relaxation time approximation is calculated. Then both the electronic thermal conductivity and the electrical conductivity divided by the relaxation time are calculated (i.e κ_e/τ and σ/τ). Experimental data have been used to determine the relaxation time as discussed in the following: The Seebeck coefficient S is independent of τ and at room temperature its experimental value is -400 $\mu V/K$ [32]. This value corresponds to the chemical potential of μ-E_F = 0.035 eV in our data of the Seebeck coefficient S versus the chemical potential at room temperature (not shown). Then, at this chemical potential (i.e. μ-E_F=0.035 eV) the electrical conductivity divided by τ (i.e σ/τ) from 100 K to 300 K is obtained from our data. Finally, it can be compared to the experimental resistivity [32] in order to extract the relaxation time. The relaxation time is a function of charge carriers and temperature which can be defined by $\tau = c/T^a n^b$ (a, b and c are three coefficients while T and n are the temperature and charge carrier densities). The three coefficients a, b and c can be obtained from three equations by considering three different temperatures and their related charge carrier densities. This leads to the values of 3, 0.69, and 1.3×10^7 $sKcm^{-1}$ for a, b, and c, respectively. Using the relaxation time $\tau = 1.3 \times 10^7/T^3 n^{0.69}$ the electrical conductivity σ and the electron thermal

conductivity κ_e for a given temperature and charge carrier density can be obtained. This treatment is different from [33].

FIG. 2a and b depict the Seebeck coefficient S and the power factor $S^2\sigma$, as a function of the chemical potential at 400 K (the positive and negative values are related to the n- and-p type doped of ZrS_xSe_{2-x}, respectively). In order to discuss the transport properties of the n and p-type doped semiconductors the rigid band approximation [3] has been widely used [4,5] in which it is assumed that for the low level doping the band structure remains unchanged. FIG. 2a and b clearly show that the Seebeck coefficient S and power factor $S^2\sigma$ in the n and p-type doped compounds can be engineered. For example, the maximum of the Seebeck coefficient in the both n and p-type ZrS_xSe_{2-x} is linearly increasing from x=0 to x=2 while opposite behavior is seen for the power factor in FIG. 2b. The maximum of the Seebeck coefficient for the n (p)-doped ZrS_2 is -2452.8 (2421.8) μV/K while for the n (p)-doped ZrSeS and $ZrSe_2$ the values of -2079.1 (2041) μV/K and -1374.5 (1332.4) μV/K, respectively have been obtained. The maximum of the power factor is observed for $ZrSe_2$ in the p-type with 1.28×10^{-3} W/mK^2 at μ-E_F =-0.031 eV (see FIG. 2b). This maximum (see FIG.2b) defines the optimum doping level to maximize the thermoelectric performance. The temperature dependence of the electrical conductivity σ, the Seebeck coefficient S, and the electronic thermal conductivity κ_e of $ZrSe_2$, ZrSeS, and ZrS_2 for the both n and p-doped cases at this optimum doping are depicted in FIG. 3. The solid and broken lines in FIG. 3 show the quantities along the a and c-crystallographic directions, respectively. In the optimal p-doped member of the three compounds the electrical conductivity σ along the a-direction is less than along the c-direction while opposite behavior is observed in the optimal n-doped of ZrS_xSe_{2-x}. This is due to the different dispersions of the CB relevant for the n-type conductivity respectively, the dispersion of the VBs relevant for p-type conductivity.

By that it can be engineered to decrease from x=0 to x=2 for the both p and n-doped ZrS_xSe_{2-x}. In all compounds (for both dopings) the absolute value of the Seebeck coefficient S decreases when increasing the temperature. The maximum of the Seebeck coefficient is observed in ZrS_2 which is 787.57 μV/K at 250 K. For all optimal p-doped compounds the electron thermal conductivity κ_e along the c-crystallographic direction is more than along the a-direction while opposite behavior is seen for the optimum n-doping.

The temperature dependence of the power factor $S^2\sigma$ at the optimum doping is depicted in FIG. 4a and b. The maximum of the power factor at 250 K for the p and n-doped of $ZrSe_2$ are 3.62×10^{-3} W/mK^2 and 3.44×10^{-3} W/mK^2, respectively. The lattice thermal conductivity of three compounds along the a and c-crystallographic directions are shown in FIG. 4c and d, respectively in which it is smaller along the c-direction than the a-direction. At 300 K the maximum lattice thermal conductivity κ_l of 3.05 W/Km is found in ZrS_2. In the three compounds at 300 K the minimum lattice thermal conductivity κ_l of 1.80 W/Km (0.26 W/Km) along the a (c)-direction is obtained for ZrSeS (with an average value of 1.28 W/Km) while it decreases to the 0.42 W/Km (0.06) W/Km at 1300 K. Here, in order to find the total thermal conductivity, it is assumed that the lattice thermal conductivity κ_l does not change at low doping level. Thus, for the optimal p-doped ZrSeS the total thermal conductivity of 1.84 W/Km (1.98 W/Km and 1.58 W/Km along the a and c-directions, respectively) at 300 K is found which decreases to 0.46 W/Km (0.61 W/Km and 0.18 W/Km along the a and c-directions, respectively) at 1000 K. It is remarkable that at 1000 K the lattice thermal conductivities along the a and c-axes in ZrSeS show the small values of 0.54 W/Km and 0.08 W/Km, respectively. The value along the c-axis is lower than the well-known low lattice thermal conductivity for SnSe which is 0.23 ± 0.03 W/Km (a-axis) at 973 K [34]. For comparison it should be noted that in SnSe the total thermal conductivities of about 0.45 W/Km, 0.69 W/Km, 0.65 W/Km for the a, c, and b-axes respectively have been reported at 300 K [34].

Previously at 300 K the lattice thermal conductivity of about 18 W/Km and 9.8 W/Km has been reported for ZrS_2 and $ZrSe_2$ [33] deviating from our corresponding values of 2.21 W/Km and 1.81 W/Km, respectively (when using a smearing of 25 cm^{-1} in the calculations). By using the non-converged smearing of 20 cm^{-1} a value of 8.93 W/Km for the lattice thermal conductivity of $ZrSe_2$ can be obtained which is close to the one reported value in Ref. [33]. But the convergence test of smearing reveals that the smearing of 20 cm^{-1} is insufficient in order to calculate the lattice thermal conductivity. The lattice thermal conductivity in Ref. [33] has been calculated by ShengBTE code [35] while the variational approaches as implemented in the QUANTUM-ESPRESSO package [6,7,17] using a robust conjugate gradient minimization has been used in our calculations. Moreover, in the QUANTUM-ESPRESSO package the anharmonic scattering coefficients among three phonons with arbitrary wave vectors are calculated based on the 2n+1 theorem within DFPT while in the ShengBTE code a real-space supercell approach has been implemented in order to calculate anharmonic interatomic force constants [35].

Since to our knowledge no experimental values for ZrS_xSe_{2-x} are reported one may check the accuracy of our method in other compounds. For example in the case of graphene [7] it has been shown that the agreement between experiment and calculations based on conjugate gradient minimization was much better than with single-mode approximation.

The figure of merit for the optimal p and-n type doped is shown in FIG. 4e and f, respectively. In the three compounds the figure of merit decreases when increasing the temperature such that its maximum is observed at 300 K in the n-doped ZrSeS compound amounting to about 0.33. Furthermore, at 300 K values of 0.31 (0.28) and 0.21 (0.22), respectively for the p (n)-doped $ZrSe_2$ and ZrS_2 have been obtained. However, in Ref. [33] the maximum figure of merit of 0.9 at about 1000 K for the n-type doped $ZrSe_2$ and 0.5 at 1400 K for the n-type doped ZrS_2 have been reported. It should be noted that in

the relaxation time equation these authors have used the exponent of 1 and 1/3 for T and n, respectively which is different from our determination presented above.

Most recently, Lv et al. [36] reported a low lattice thermal conductivity of 3.29 W/Km and an optimized ZT of 1.6 at 300 K in monolayer ZrS_2. Also, a low optimized ZT of about 0.1 at 1200 K in monolayer $MoSe_2$ [37] was found. For a monolayer of MoS_2, a value of about 0.11 at 500 K was obtained by Jin et al. [38]. Monolayer WSe_2 exhibited a value of ZT about 0.7 at high temperature [37]. In our calculation the optimum ZT value is interestingly obtained for the mixed crystal which reveals the lowest lattice thermal conductivity. Lower lattice thermal conductivity is playing a major role in order to increase the ZT as has also been found in this study, while the power factor of $ZrSe_2$ is higher than that of ZrSeS and ZrS_2 but the lower lattice thermal conductivity of ZrSeS results in the highest ZT.

4. Conclusion

In summary, the band structure, DOS, phonon dispersion, and transport properties of the ternary ZrS_xSe_{2-x} (x=0, 1, and 2) have been calculated. Using two methods for engineering the transport properties - doping and the substitution of S by Se in ZrS_xSe_{2-x} (x=0.1, 2) - enables us to look at the optimal transport properties of each compound. As a result the highest figure of merit ZT is observed for ZrSeS, while $ZrSe_2$ reveals the highest power factor and lowest bandgap. We report on the minimum total (lattice) thermal conductivity in ZrSeS of 0.61 W/Km (0.54 W/Km) and 0.18 W/Km (0.08 W/Km) along the a and c-directions, respectively at 1000 K. This value of the lattice thermal conductivity along the c-axis is lower than the reported value for SnSe [2].

ACKNOWLEDGMENTS

All calculations in this paper have been performed at the Helmholtz-Zentrum Berlin (HZB). A. Ghafari gratefully thanks Dr. Klaus Habicht for support and discussion as well as wishes to express his appreciation to the computational facility and support at the HZB.

Data availability

The raw/processed data required to reproduce these findings cannot be shared at this time as the data also forms part of an ongoing study.

References

[1] G.J. Snyder, E.S. Toberer, Complex thermoelectric materials, Nat. Mater. 7 (2008) 105–114. doi:10.1038/nmat2090.
[2] X. Zhang, L.-D. Zhao, Thermoelectric materials: Energy conversion between heat and electricity, J. Mater. 1 (2015) 92–105. doi:10.1016/j.jmat.2015.01.001.
[3] A. Stern, Rigid-Band Model of, Phys. Rev. 157 (1967) 544–551.
[4] K. Kutorasinski, B. Wiendlocha, S. Kaprzyk, J. Tobola, Electronic structure and thermoelectric properties of n-and p-type SnSe from first-principles calculations, Phys. Rev. B. 91 (2015) 205201. doi:10.1103/PhysRevB.91.205201.
[5] A.J. Hong, L. Li, H.X. Zhu, Z.B. Yan, J.-M. Liu, Z.F. Ren, Optimizing the thermoelectric performance of low-temperature SnSe compounds by electronic structure design, J. Mater. Chem. A. 3 (2015) 13365–13370. doi:10.1039/C5TA01703C.
[6] G. Fugallo, M. Lazzeri, L. Paulatto, F. Mauri, Ab initio variational approach for evaluating lattice thermal conductivity, Phys. Rev. B. 88 (2013) 045430. doi:10.1103/PhysRevB.88.045430.
[7] L. Paulatto, F. Mauri, M. Lazzeri, Anharmonic properties from a generalized third-order ab initio approach: Theory and applications to graphite and graphene, Phys. Rev. B. 87 (2013) 214303. doi:10.1103/PhysRevB.87.214303.
[8] M. Moustafa, T. Zandt, C. Janowitz, R. Manzke, Growth and band gap determination of the ZrSxSe2−x single crystal series, Phys. Rev. B. 80 (2009) 035206. doi:10.1103/PhysRevB.80.035206.
[9] M. Moustafa, A. Paulheim, M. Mohamed, C. Janowitz, R. Manzke, Angle-resolved photoemission studies of the valence bands of ZrS x Se 2−x, Appl. Surf. Sci. 366 (2016) 397–403. doi:10.1016/j.apsusc.2016.01.024.
[10] M. Moustafa, A. Ghafari, A. Paulheim, C. Janowitz, R. Manzke, Spin orbit splitting in the valence bands of ZrSxSe2−x: Angle resolved photoemission and density functional theory, J. Electron Spectros. Relat. Phenomena. 189 (2013) 35–39. doi:10.1016/j.elspec.2012.12.010.
[11] A. Ghafari, A. Boochani, C. Janowitz, R. Manzke, Electronic structure of ZrSxSe2−x by Tran-Blaha modified Becke-Johnson density functional, Phys. Rev. B. 84 (2011) 125205. doi:10.1103/PhysRevB.84.125205.
[12] A. Ghafari, C. Janowitz, R. Manzke, The effect of lithium intercalation on the electronic structure of the ternary compound semiconductors ZrSe 2− x S x, J. Phys. Condens. Matter. 25 (2013) 315502. doi:10.1088/0953-8984/25/31/315502.
[13] A. Ghafari, M. Moustafa, G. Di Santo, L. Petaccia, C. Janowitz, Opposite dispersion bands at the Fermi level in ZrSe 2, Appl. Phys. Lett. 112 (2018) 182105. doi:10.1063/1.5025794.
[14] S.G. Patel, S.K. Arora, M.K. Agarwal, CVT growth of zirconium sulphoselenide single crystals, Bull. Mater. Sci. 21 (1998) 297–301. doi:10.1007/BF02744956.
[15] P. Blaha, K. Schwarz, P. Sorantin, S.B. Trickey, Full-potential, linearized augmented plane wave programs for crystalline systems, Comput. Phys. Commun. 59 (1990) 399–415. doi:10.1016/0010-4655(90)90187-6.
[16] J.P. Perdew, A. Ruzsinszky, G.I. Csonka, O.A. Vydrov, G.E. Scuseria, V.N. Staroverov, J. Tao, Exchange and correlation in open systems of fluctuating electron number, Phys. Rev. A. 76 (2007) 040501. doi:10.1103/PhysRevA.76.040501.
[17] P. Giannozzi, S. Baroni, N. Bonini, M. Calandra, R. Car, C. Cavazzoni, D. Ceresoli, G.L. Chiarotti, M. Cococcioni, I. Dabo, A. Dal Corso, S. de Gironcoli, S. Fabris, G. Fratesi, R. Gebauer, U. Gerstmann, C. Gougoussis, A. Kokalj, M. Lazzeri, L. Martin-Samos, N. Marzari, F. Mauri, R. Mazzarello, S. Paolini, A. Pasquarello, L. Paulatto, C. Sbraccia, S. Scandolo, G. Sclauzero, A.P. Seitsonen, A. Smogunov, P. Umari, R.M. Wentzcovitch, QUANTUM ESPRESSO: a modular and open-source software project for quantum simulations of materials, J. Phys. Condens. Matter. 21 (2009) 395502. doi:10.1088/0953-8984/21/39/395502.

[18] A. Debernardi, S. Baroni, E. Molinari, Anharmonic Phonon Lifetimes in Semiconductors from Density-Functional Perturbation Theory, Phys. Rev. Lett. 75 (1995) 1819–1822. doi:10.1103/PhysRevLett.75.1819.
[19] M. Lazzeri, S. de Gironcoli, First-principles study of the thermal expansion of Be(101¯0) Michele, Phys. Rev. B. 65 (2002) 245402. doi:10.1103/PhysRevB.65.245402.
[20] G. Deinzer, G. Birner, D. Strauch, Ab initio calculation of the linewidth of various phonon modes in germanium and silicon, Phys. Rev. B. 67 (2003) 144304. doi:10.1103/PhysRevB.67.144304.
[21] J.P. Perdew, K. Burke, M. Ernzerhof, Generalized Gradient Approximation Made Simple, Phys. Rev. Lett. 77 (1996) 3865–3868. doi:10.1103/PhysRevLett.77.3865.
[22] G.K.H. Madsen, D.J. Singh, BoltzTraP. A code for calculating band-structure dependent quantities, Comput. Phys. Commun. 175 (2006) 67–71. doi:10.1016/j.cpc.2006.03.007.
[23] F. Tran, P. Blaha, Accurate Band Gaps of Semiconductors and Insulators with a Semilocal Exchange-Correlation Potential, Phys. Rev. Lett. 102 (2009) 226401. doi:10.1103/PhysRevLett.102.226401.
[24] J.P. Perdew, M. Ernzerhof, K. Burke, Rationale for mixing exact exchange with density functional approximations, J. Chem. Phys. 105 (1996) 9982–9985. doi:10.1063/1.472933.
[25] A.D. Becke, Density-functional thermochemistry. III. The role of exact exchange, J. Chem. Phys. 98 (1993) 5648–5652. doi:10.1063/1.464913.
[26] R. Ahlrichs, M. Bär, M. Häser, H. Horn, C. Kölmel, Electronic structure calculations on workstation computers: The program system turbomole, Chem. Phys. Lett. 162 (1989) 165–169. doi:10.1016/0009-2614(89)85118-8.
[27] A. Ghafari, L. Petaccia, C. Janowitz, Splitting of the Ti-3d bands of TiSe 2 in the charge-density wave phase, Appl. Surf. Sci. 396 (2017) 1649–1656. doi:10.1016/j.apsusc.2016.12.016.
[28] A. Ghafari, C. Janowitz, The role of out of plane orbitals in the electronic properties of undoped Ca x Sr 1 − x CuO 2, Comput. Mater. Sci. 127 (2017) 78–84. doi:10.1016/j.commatsci.2016.10.026.
[29] R.P. CHASMAR, R. STRATTON, The Thermoelectric Figure of Merit and its Relation to Thermoelectric Generators†, J. Electron. Control. 7 (1959) 52–72. doi:10.1080/00207215908937186.
[30] G.D. Mahan, Figure of merit for thermoelectrics, J. Appl. Phys. 65 (1989) 1578–1583. doi:10.1063/1.342976.
[31] P.C. Klipstein, C.M. Pereira, R.H. Friend, Transport and Raman studies of the group IV layered compounds and their lithium intercalates: Li x TiS 2 , Li x TiSe 2 , Li x ZrS 2 , Li x ZrSe 2 , Li x HfS 2 and Li x HfSe 2, Philos. Mag. B. 56 (1987) 531–559. doi:10.1080/13642818708220162.
[32] T.C. Holgate, Y. Liu, D. Hitchcock, T.M. Tritt, J. He, Thermoelectric Properties of Li-Intercalated ZrSe2 Single Crystals, J. Electron. Mater. 42 (2013) 1751–1755. doi:10.1007/s11664-012-2410-1.
[33] G. Yumnam, T. Pandey, A.K. Singh, High temperature thermoelectric properties of Zr and Hf based transition metal dichalcogenides: A first principles study, J. Chem. Phys. 143 (2015) 234704. doi:10.1063/1.4937774.
[34] L.-D. Zhao, S.-H. Lo, Y. Zhang, H. Sun, G. Tan, C. Uher, C. Wolverton, V.P. Dravid, M.G. Kanatzidis, Ultralow thermal conductivity and high thermoelectric figure of merit in SnSe crystals, Nature. 508 (2014) 373–377. doi:10.1038/nature13184.
[35] W. Li, J. Carrete, N. A. Katcho, N. Mingo, ShengBTE: A solver of the Boltzmann transport equation for phonons, Comput. Phys. Commun. 185 (2014) 1747–1758. doi:10.1016/j.cpc.2014.02.015.
[36] H.Y. Lv, W.J. Lu, D.F. Shao, H.Y. Lu, Y.P. Sun, Strain-induced enhancement in the

thermoelectric performance of a ZrS 2 monolayer, J. Mater. Chem. C. 4 (2016) 4538–4545. doi:10.1039/C6TC01135G.
[37] S. Kumar, U. Schwingenschlögl, Thermoelectric Response of Bulk and Monolayer MoSe 2 and WSe 2, Chem. Mater. 27 (2015) 1278–1284. doi:10.1021/cm504244b.
[38] Z. Jin, Q. Liao, H. Fang, Z. Liu, W. Liu, Z. Ding, T. Luo, N. Yang, A Revisit to High Thermoelectric Performance of Single-layer MoS 2, Sci. Rep. 5 (2016) 18342. doi:10.1038/srep18342.
[39] L. Roubi, C. Carlone, Resonance Raman spectrum of HfS2 and ZrS2, Phys. Rev. B. 37 (1988) 6808–6812. doi:10.1103/PhysRevB.37.6808.

Table 1. Comparison of the indirect band gap of ZrS_xSe_{2-x} (x=0, 1, 2) structures between the $E_{\Gamma L}$ and $E_{\Gamma M}$ by B3LYP, PBE0, and MBJ (with SO and WSO interaction). The $E_{\Gamma M}$ band gaps are presented in parenthesis. The energy units are electron volt.

Functional	$ZrSe_2$	ZrSeS	ZrS_2
B3LYP	0.965 (1.147)	1.201 (1.396)	1.452 (1.634)
PBE0	1.066 (1.258)	1.323 (1.518)	1.594 (1.778)
MBJ	0.927 (0.751)	1.297 (1.008)	1.422 (1.026)
MBJSO	0.642 (0.818)	0.960 (1.136)	1.255 (1.415)
Experimental [a]	1.18	1.4	1.70
Experimental [b]	1.10	-	2.02

[a] Optical absorption measurements [8]

[b] ARPES [9]

Table 2. Comparison of the direct band gap of ZrS_xSe_{2-x} (x=0, 1, 2) at the Γ, A, L, and M-points by B3LYP, PBE0, and MBJ (with SO and WSO interaction). The energy units are electron volt.

Functional	$ZrSe_2$				ZrSeS				ZrS_2			
	E_Γ	E_A	E_L	E_M	E_Γ	E_A	E_L	E_M	E_Γ	E_A	E_L	E_M
B3LYP	1.655	1.869	2.007	2.637	1.944	2.163	2.155	2.823	2.161	2.510	2.344	3.124
PBE0	1.824	2.035	2.178	2.811	2.126	2.343	2.333	3.005	2.353	2.698	2.533	3.323
MBJ	1.349	1.580	1.699	2.287	1.640	1.882	1.862	2.481	1.850	2.231	2.063	2.790
MBJSO	1.236	1.440	1.614	1.450	1.584	1.793	1.822	2.471	1.841	2.193	2.056	2.788
Exp. [a]		1.61				1.80				2.10		

[a] Optical absorption measurements for direct band gap [8]

Table 3. Frequencies of Raman active modes for ZrS_xSe_{2-x} (x=0, 1, 2). The E_g and A_{1g} are the in-plane and out-of-plane mode vibrations.

	E_g		A_{1g}	
system	Cal.	Exp.	Cal.	Exp.
$ZrSe_2$	149.36 (146.46 [a])	145.5 [b]	193.29 (202.57 [a])	194.50 [b]
ZrSeS	199.79	-	239.43	-
ZrS_2	253.61 (255.46 [a])	250 [b] (251±2) [c]	338.50 (334.78 [a])	334.1 [b] (333±2) [c]

[a] Ref. [33]

[b] Ref. [31]

[c] Ref. [39]

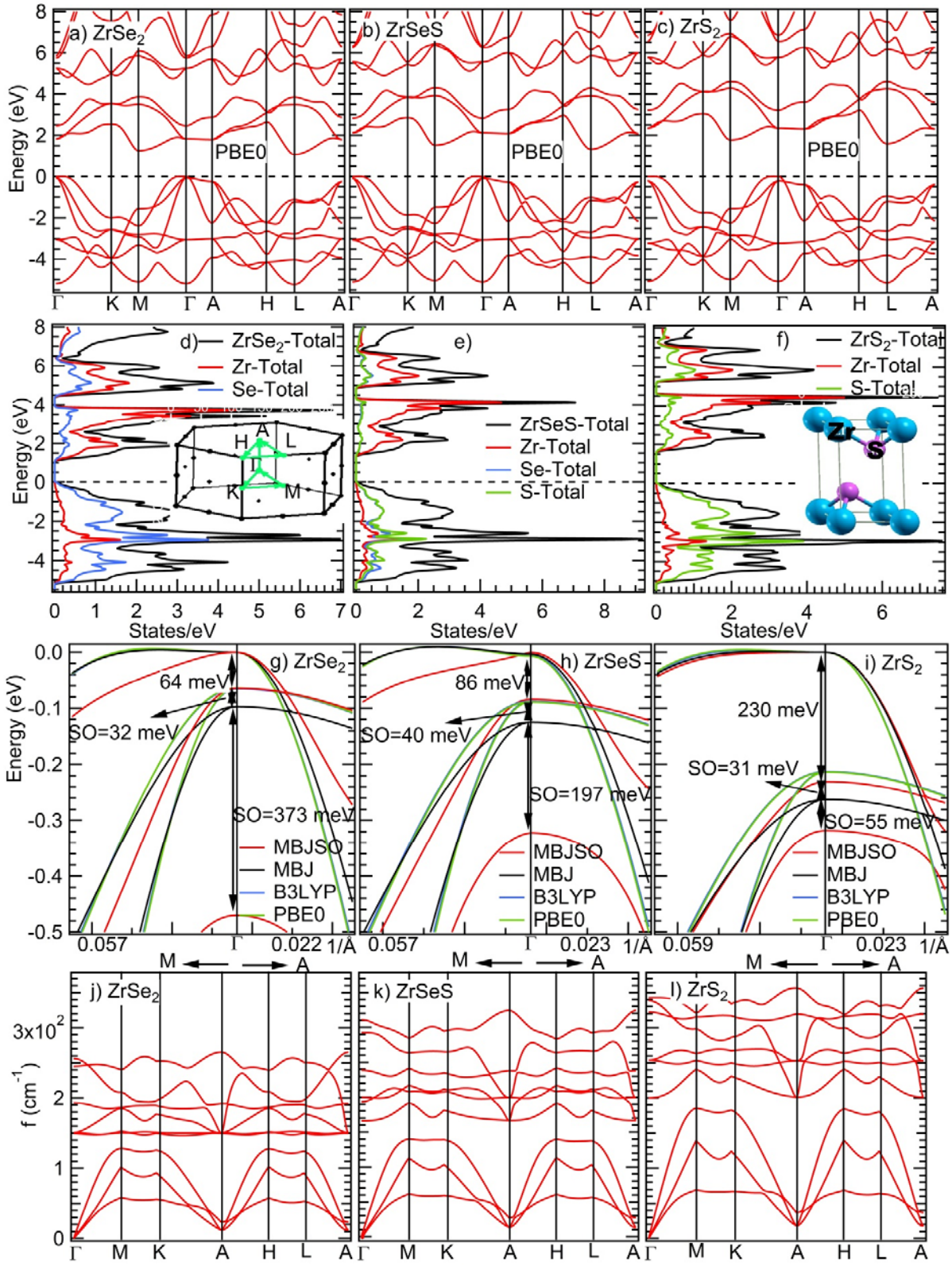

FIG. 1: Band structures of the ternary ZrS_xSe_{2-x} calculated using the PBE0 hybrid functional are presented in (a), (b), and (c), respectively for x=0, 1, and 2. Total DOS and partial DOS of ZrS_xSe_{2-x} are

shown in (d)-(f). The inset in (d) and (f) show the Brillouin zone, and crystal structure, respectively. Zoom into the dispersion of bands at the Γ-point close to the top third of the VBM of $ZrSe_2$, ZrSeS and ZrS_2 are depicted in (g)-(i), respectively. Phonon spectra of the ternary ZrS_xSe_{2-x} (x=0, 1, 2) around high symmetrical points of the BZ are shown in (j)-(l), respectively.

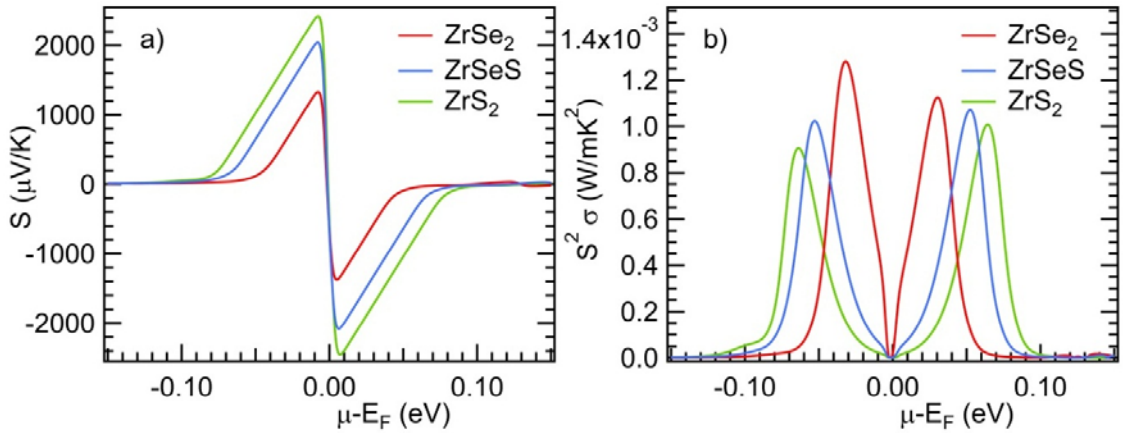

FIG. 2: The Seebeck coefficient S and power factor $S^2\sigma$ as a function of the chemical potential at 400 K are shown in a and b, respectively. The positive and negative values correspond to the n and-p type doped regime.

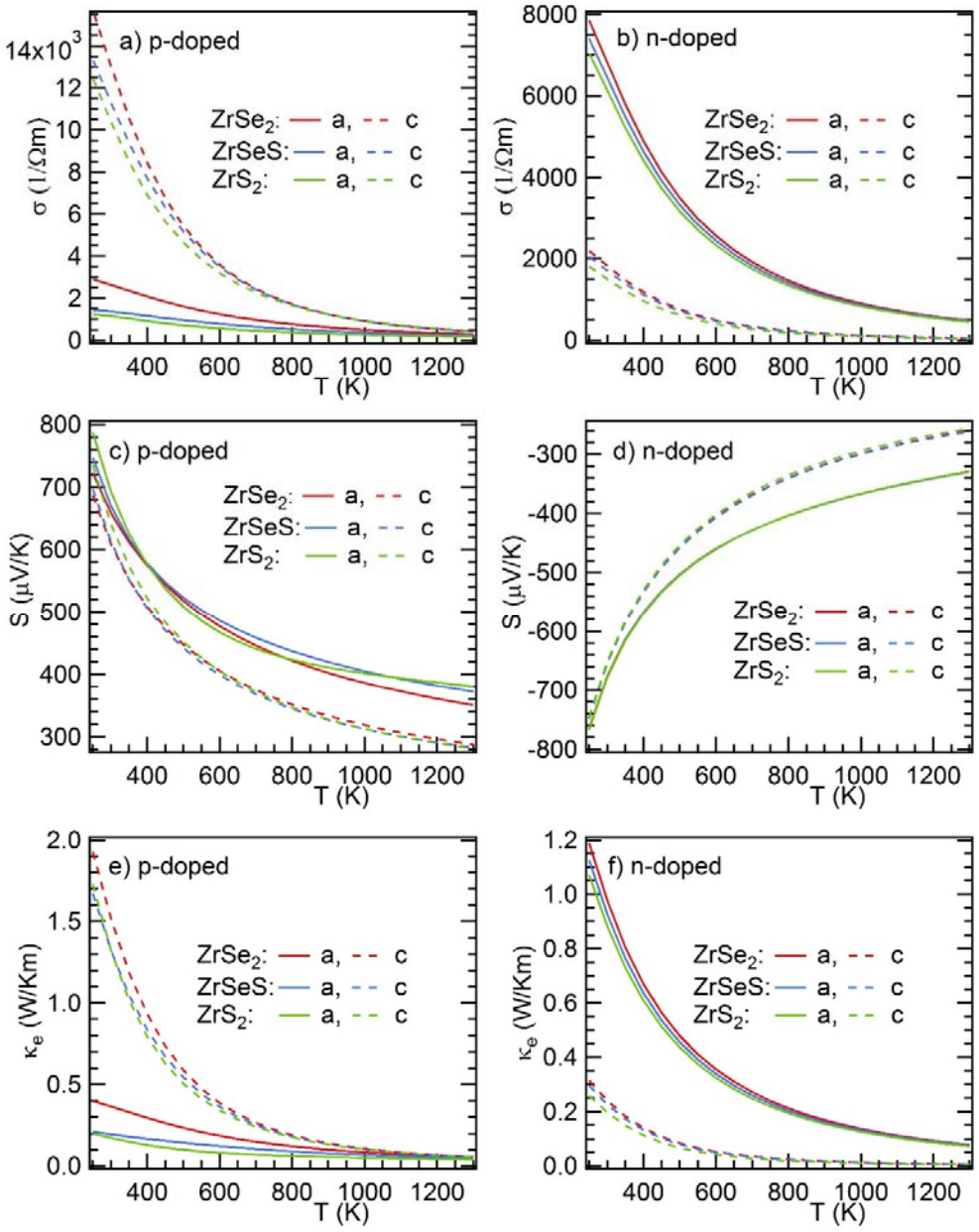

FIG. 3: a (b), c (d), and e (f) respectively, the electrical conductivity σ, the Seebeck coefficient S, and the electronic thermal conductivity κ_e at the optimal p (n)-doped as a function of temperature for $ZrSe_2$, ZrSeS, and ZrS_2. The solid and dashed lines show the values along the a and c-crystallographic directions, respectively.

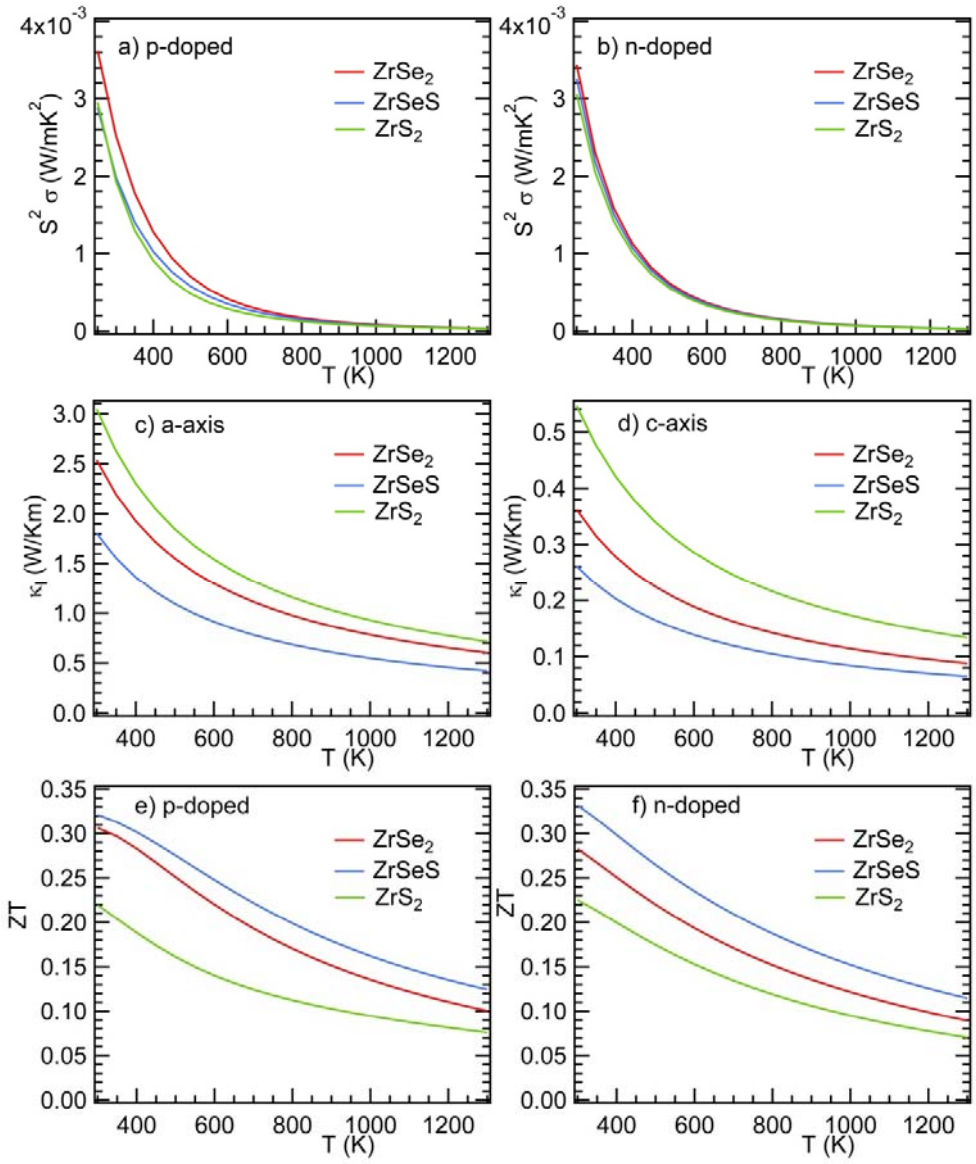

FIG. 4: In a (b) and e (f) respectively, the power factor $S^2\sigma$ and the figure of merit ZT as a function of temperature for the optimal p (n)-doped of $ZrSe_2$, ZrSeS, and ZrS_2 and in c and d the lattice thermal conductivity as a function of temperature along the a and c-crystallographic directions, respectively is depicted.